

# QCD Instanton-induced Processes in Deep-inelastic Scattering - Search Strategies and Model Dependencies\*

T. Carli<sup>a</sup>, J. Gerigk<sup>a</sup>, A. Ringwald<sup>b</sup> and F. Schrempp<sup>b</sup>

<sup>a</sup> Max-Planck-Institut für Physik, München, Germany

<sup>b</sup> Deutsches Elektronen-Synchrotron DESY, Hamburg, Germany

## Abstract

We investigate possible search strategies for QCD-instanton induced processes at HERA in the deep-inelastic scattering (DIS) regime. Our study is based on the Monte Carlo generator QCDINS for instanton-induced events and the standard generators for normal DIS events. It appears possible to isolate an instanton enriched data sample via an optimized multi-dimensional cut scenario for a set of six most instanton-sensitive DIS observables. As a further central point, we investigate the stability of our results with respect to a variation of the (hadronization) models available for the simulation of both normal DIS and instanton-induced events. Dependencies on the variation of certain inherent parameters are also studied. Within the “bandwidth” of variations considered, we find that the normal DIS background is typically much more sensitive to model variations than the I-induced signal.

---

\*Contribution to the Proceedings of the DESY Workshop 1998/99 on Monte Carlo Generators for HERA Physics.

# 1 Introduction

Instantons (I) have been known to theoretical physics since the mid seventies [1, 2, 3, 4]. They represent non-perturbative fluctuations of the gauge fields in non-Abelian theories like QCD and weak interactions, associated with tunneling transitions between degenerate ground states (vacua) of different topology.

Instanton transitions induce processes [2, 3, 4] violating the (classical) conservation of certain fermionic quantum numbers, namely chirality in QCD and the sum of baryon and lepton number in weak interactions. These processes are forbidden in ordinary perturbation theory, but have to exist in general due to the famous ABJ chiral anomaly [5, 6, 7].

The DIS regime at HERA offers a unique possible discovery window for events induced by QCD-instantons through their characteristic final state signature [8, 9, 10, 11, 12] and a sizable rate, calculable<sup>1</sup> within I-perturbation theory [14, 15, 16]. An experimental detection of these processes would correspond to a novel, non-perturbative manifestation of non-Abelian gauge theories and would clearly be of basic significance.

This report is organized as follows<sup>2</sup>:

We start off in section 2 by introducing the dominant I-induced DIS process along with the relevant kinematics. Then we proceed by summarizing the essential ingredients and the basic structure of the Monte Carlo generator QCDINS for instanton-induced DIS events [9, 18], on which the present study is based. In section 3, we recall the theoretical results for the I-induced cross section at HERA and summarize the corresponding characteristic topology of the hadronic final state. Section 4 is devoted to a study of the possibility to reconstruct the Bjorken variables of the I-subprocess. Sections 5 and 6 contain the central results of this investigation. In Section 5, we report on a possible search strategy for these processes. The goal is to isolate an instanton enriched data sample via an optimized multi-dimensional cut scenario for a set of most I-sensitive DIS observables. Finally, in section 6, we investigate the stability of our results with respect to a variation of the (hadronization) models available for the simulation of both normal DIS and instanton-induced events. Dependencies on the variation of certain inherent parameters are also considered.

All the studies presented in this report are performed in the hadronic center of mass frame<sup>3</sup> (hCMS), which is a suitable frame of reference in view of a good distinction between I-induced and normal DIS events (c.f. [12]). The results that we obtain are based on a study of the hadronic final state, with typical acceptance cuts of a HERA detector being applied in the laboratory frame ( $15^\circ < \Theta_{hadron} < 155^\circ$  and  $p_T(hadron) > 0.15$  GeV, for charged particles,  $\Theta_{hadron} > 4^\circ$ , for all stable particles, and  $0.25 < p_T^2(K^0) < 4.5$  GeV<sup>2</sup>, for neutral kaons)<sup>4</sup>.

---

<sup>1</sup>For an exploratory calculation of the I-contribution to the gluon structure function see Ref. [13].

<sup>2</sup>An extended version of this paper will appear elsewhere [17].

<sup>3</sup>This frame is defined by  $\vec{q} + \vec{P} = \vec{0}$ . Therefore, the photon and the incoming proton collide head-on.

<sup>4</sup> In the laboratory frame the incoming proton points in the positive z-direction, while in the hCMS the proton points in the negative z-direction.

## 2 The Monte Carlo Generator QCDINS

In deep-inelastic  $e^\pm P$  scattering, I-induced events are predominantly associated with a process structure as sketched in Fig. 1: A photon splitting into a quark-antiquark pair, fuses with a gluon from the proton in the background of an instanton or an anti-instanton. Besides the current-quark (jet), the partonic final state consists of  $2n_f - 1$  right (left)-handed (massless) quarks and anti-quarks and  $n_g$  gluons emitted by the instanton (anti-instanton). Correspondingly, the total violation of *chirality*  $\equiv \#q_R - \#q_L$  is  $\pm 2n_f$ , in agreement with the ABJ chiral anomaly relation [5, 6, 7].

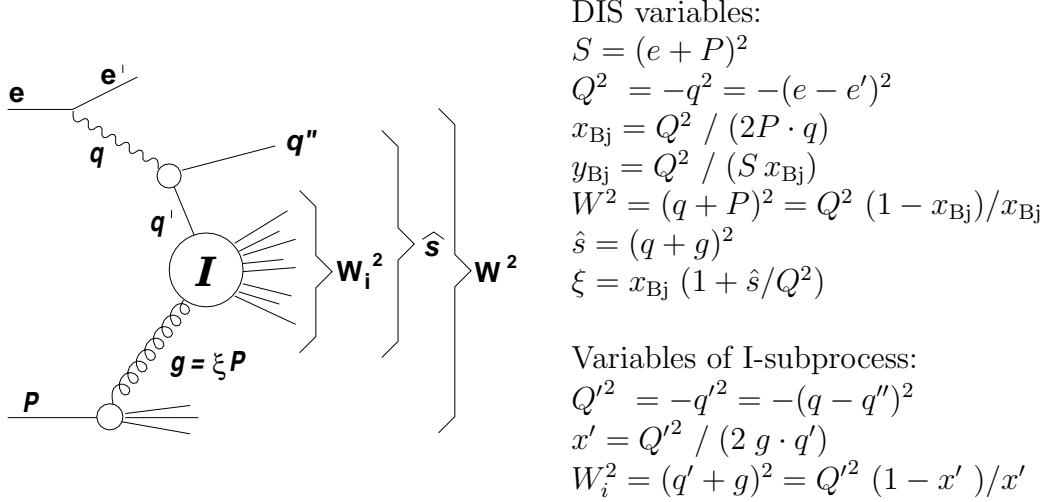


**Figure 1:** Kinematic variables of the dominant I-induced process in deep-inelastic scattering.

I-induced processes initiated by a quark from the proton are suppressed by a factor of  $\alpha_s^2$  with respect to the gluon initiated process [15]. This fact together with the high gluon density in the relevant kinematical domain at HERA, justifies to neglect quark initiated processes.

QCDINS [9, 18] is a Monte Carlo package for simulating QCD-instanton induced scattering processes in DIS. It is designed as an “add-on” hard process generator interfaced by default to the Monte Carlo generator HERWIG [19].

QCDINS incorporates the essential characteristics, that have been derived theoretically for the hadronic final state of I-induced processes: notably, the *isotropic* production of the partonic final state in the I-rest system ( $q'g$  CMS in Fig. 1), flavour “democracy”, energy weight factors different for gluons and quarks, and a high average multiplicity  $2n_f + \mathcal{O}(1/\alpha_s)$  of produced partons with a (approximate) Poisson distribution of the gluon multiplicity.

Let us briefly summarize the main stages involved in QCDINS, to generate the complete I-induced partonic final state in DIS.

The first stage is the generation of the various Bjorken variables (c.f. Fig. 1) of the I-induced DIS process. They are generated in the order  $Q'^2, x', \xi, x_{Bj}, y_{Bj}$ , with weights corresponding to the

I-induced total cross section [15, 16],

$$d\sigma_{eP}^{(I)} \simeq \frac{2\pi\alpha^2 e_{q'}^2}{S} dQ'^2 \frac{dx'}{x'} \frac{\sigma_{q'g}^{(I)}(x', Q'^2)}{x'} \frac{d\xi}{\xi} f_g(\xi) \frac{dx_{\text{Bj}}}{x_{\text{Bj}}} \frac{dy_{\text{Bj}}}{y_{\text{Bj}}} \frac{1 + (1 - y_{\text{Bj}})^2}{y_{\text{Bj}}} P_{q'}^{(I)}, \quad (1)$$

subject to appropriate kinematical restrictions (e. g.  $0 \leq x_{\text{Bj}} \leq x_{\text{Bj}}/\xi \leq x' \leq 1$ ) and fiducial cuts. Here  $e_{q'}^2$  denotes the electric charge squared of the virtual quark  $q'$  in units of the electric charge squared,  $e^2 = 4\pi\alpha$ , and  $f_g$  is the gluon density in the proton. The weight factor  $P_{q'}^{(I)}$  accounts for the flux of virtual quarks  $q'$  in the I-background [15, 16],

$$P_{q'}^{(I)} = \frac{3}{16\pi^3} \frac{x_{\text{Bj}}}{\xi x'} \left( 1 + \frac{\xi}{x_{\text{Bj}}} - \frac{1}{x'} - \frac{Q'^2}{Sx_{\text{Bj}}y_{\text{Bj}}} \right). \quad (2)$$

In Eq. (1), the I-induced  $q'g$ -subprocess total cross section  $\sigma_{q'g}^{(I)}$  contains the essential instanton dynamics [15]. As illustrated in Fig. 2, it is very steeply growing for decreasing values of  $Q'^2$  and

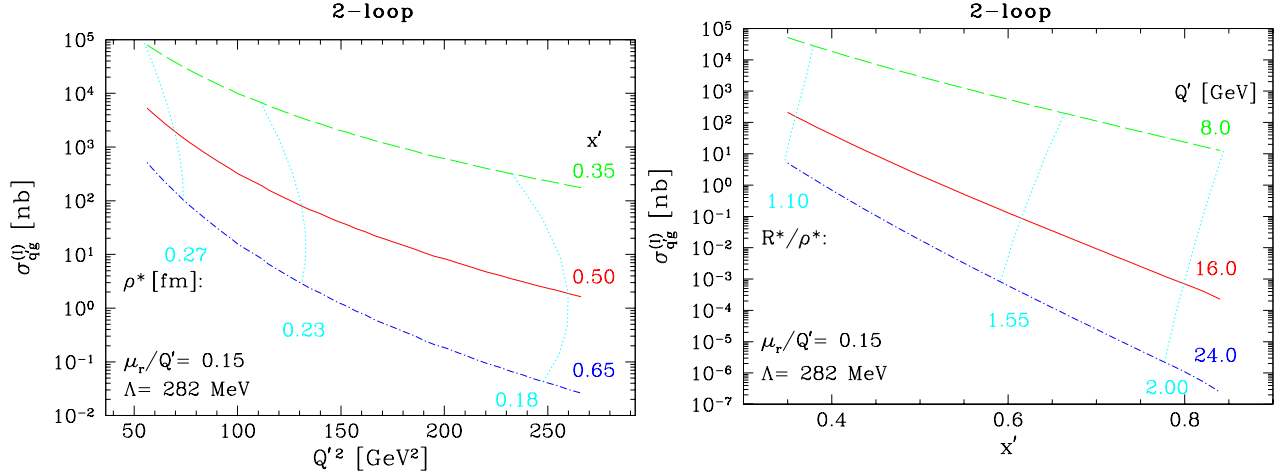


**Figure 2:** I-subprocess cross section [15] displayed versus the Bjorken variable  $Q'^2$  with  $x'$  fixed (left) and versus  $x'$  with  $Q'^2$  fixed (right) for  $n_f = 3$ . The dotted lines indicate the corresponding effective  $I$ -sizes  $\rho^*$  [fm] (left) and  $I\bar{I}$ -distances  $R^*$  in units of  $\rho^*$  (right), respectively.

$x'$ , respectively. In order to remain within the region of validity of I-perturbation theory [15, 20], the following cuts are implemented by default in QCDINS,

$$Q'^2 \geq Q'^2_{\min} = 64 \text{ GeV}^2; \quad x' \geq x'_{\min} = 0.35. \quad (3)$$

An additional cut on the photon virtuality,

$$Sx_{\text{Bj}}y_{\text{Bj}} \equiv Q^2 \geq Q^2_{\min} = 64 \text{ GeV}^2, \quad (4)$$

should in principle be applied in order to warrant sufficient suppression of non-planar contributions [14], which may spoil the validity of Eq. (1). The cross section  $\sigma_{q'g}^{(I)}$  depends strongly on the

QCD scale  $\Lambda_{\overline{\text{MS}}}^{(n_f)}$  and weakly on the renormalization scale  $\mu_r$ . By default, these scales are taken as

$$\Lambda_{\overline{\text{MS}}}^{(3)} = 0.282 \text{ GeV}; \quad \mu_r = 0.15 Q'. \quad (5)$$

Note that strictly speaking, the underlying theoretical framework refers to massless quarks. Therefore, the (default) number of flavours was set to  $n_f = 3$  and  $\Lambda_{\overline{\text{MS}}}^{(3)}$  in Eq. (5) was obtained by a standard flavour reduction from the DIS average,  $\Lambda_{\overline{\text{MS}}}^{(4)} = 234 \text{ MeV}$  in Ref. [21]. The default value for  $\mu_r$  above corresponds to the minimum [15],  $\partial\sigma_{q'g}/\partial\mu_r = 0$ .

In the second stage of the event generation, the 4-momenta  $g, q, q', q''$  of the incoming gluon  $g$ , the virtual photon  $q$ , the virtual quark  $q'$  and the current quark  $q''$ , respectively, are filled. Sudakov decompositions of these momenta are used to incorporate various constraints, e.g. on the momenta squared,  $g^2 = m_g^2 (= (0.75 \text{ GeV})^2 \text{ by default})$ ,  $q^2 = -Q^2$ ,  $q'^2 = -Q'^2$ ,  $q''^2 = m_{q''}^2$ . The 4-momentum of the outgoing lepton,  $e'$ , is calculated subsequently.

In the third stage, the partonic final state of the I-induced  $q'g$ -subprocess is generated in the  $q'g$  CMS as follows. The number  $n_g$  of produced gluons is generated according to a Poisson distribution with mean  $\langle n_g \rangle^{(I)} \sim 1/\alpha_s \sim 3$  as calculated theoretically in I-perturbation theory.  $n_f (= 3)$   $[q \dots \bar{q}]$  - “strings” of partons are set up, each beginning with a quark, followed by a random number of gluons and ending with an anti-quark of randomly chosen flavour. There are  $n_g + 1$  gluons in total and all  $n_f$  flavours occur precisely once. A simple example for  $n_g = 3$  outgoing gluons may provide some illustration:  $[u \ g \ g \ \bar{s}] [d \ g \ \bar{u}] [s \ g \ g \ \bar{d}]$ . A quark and a gluon among these  $2n_f + n_g + 1$  partons are (randomly) marked as incoming.

The momenta  $p_i$  of the  $n = 2n_f - 1 + n_g$  outgoing partons in the instanton subprocess CMS are then generated according to the energy-weighted phase-space distribution

$$\begin{aligned} & \int \prod_{i=1}^{2n_f-1} \{d^4 p_i \delta(p_i^2 - m_i^2) p_i^0\} \prod_{k=1}^{n_g} \{d^4 p_k \delta(p_k^2 - m_g^2) p_k^{0,2}\} \\ & \times \delta^{(3)} \left( \sum_{i=1}^{2n_f-1} \vec{p}_i + \sum_{k=1}^{n_g} \vec{p}_k \right) \delta \left( W_i - \sum_{i=1}^{2n_f-1} p_i^0 - \sum_{k=1}^{n_g} p_k^0 \right), \end{aligned} \quad (6)$$

corresponding to the leading-order matrix element with different energy weights for gluons and quarks.

Next, the colour and flavour connections of the partons are set up. The colour flow is obtained simply by connecting the colour lines of neighbouring partons within each of the above-mentioned  $n_f [q \dots \bar{q}]$  - “strings” in a planar manner (consistent with the leading order  $1/N_c$  expectation).

The partonic stage of the event generation ends by boosting the momenta of the I-subprocess final state partons to the laboratory frame.

After the perturbative evolution of the generated partons, one may use the hadronization mechanisms inherent in various Monte Carlo models (e.g. HERWIG [19] or JETSET [22]) to arrive at the complete hadronic final state.

### 3 Cross section and Signature

The total cross section of I-induced events in DIS, calculated within I-perturbation theory, is surprisingly large. For  $x_{Bj} \geq 10^{-3}$  and  $0.1 < y_{Bj} < 0.9$ , the result of Ref. [15] is

$$\sigma_{HERA}^{(I)}(x' \geq 0.35; Q' \geq 8 \text{ GeV}) \simeq 130 \text{ pb.} \quad (7)$$

Hence, given the total integrated luminosity  $\mathcal{L} \simeq 30 \text{ pb}^{-1}$  accumulated by each of the HERA experiments in the years 1996/1997, in this kinematical region a large number  $N = \sigma_{HERA}^{(I)} \cdot \mathcal{L} = \mathcal{O}(10^4)$  of I-induced events should already have been taken on tape.

The cross section (7) corresponds to a fraction of I-induced to normal DIS (nDIS) events of [15]

$$f^{(I)} = \frac{\sigma_{HERA}^{(I)}}{\sigma_{HERA}^{(nDIS)}} = \mathcal{O}(1)\%. \quad (8)$$

However, this prediction for the cross section still contains considerable uncertainties [15]. One of the dominant ones arises from the experimental uncertainty of  $\pm 65 \text{ MeV}$  associated with the QCD scale  $\Lambda_{\overline{\text{MS}}}^{(3)}$  in Eq. (5). If  $\Lambda_{\overline{\text{MS}}}^{(3)}$  is varied within the allowed range of  $\pm 65 \text{ MeV}$ , the cross section varies by  $\mathcal{O}(+300) \text{ pb}$  and  $\mathcal{O}(-100) \text{ pb}$ , respectively.

By far the dominant uncertainty, however, comes in principle from the choice of the lower bounds on  $x'$  and  $Q'$ , due to the strong increase of the I-subprocess cross section with decreasing values of the cuts  $x'_{min}$  and  $Q'_{min}$ , respectively (cf. Fig. 2). However, recent high-quality “data” from a (non-perturbative) lattice simulation [23] on the topological structure of the QCD vacuum have strongly reduced this uncertainty. The lattice results could be directly converted into a “fiducial”  $(x', Q')$  region, where the predictions from I-perturbation theory should (approximately) hold [20]. The lower bounds on  $x'$  and  $Q'$  given in Eq. (7) correspond to this fiducial region and are thus expected to be quite reliable .

Let us next turn to the expected signature of the I-induced final state.

Fig. 3a shows the transverse energy distribution in the  $\eta^*-\Phi$  plane of a “typical” I-induced event in DIS, produced by the instanton Monte Carlo generator QCDINS [9, 18]. There are the following characteristics:

- **Topology: “Instanton band” and current jet**

In the instanton CMS (the  $q'g$  CMS, cf. Fig. 1) the production of partons coming from the I-subprocess is isotropic. This leads to an energy distribution of hadrons restricted to a certain range in the pseudo-rapidity  $\eta$  (the “instanton-band”) with a bandwidth of  $\simeq \pm 1.1$  units in  $\eta$ . In the instanton CMS this band is localized around  $\eta = 0$ , while in the hCMS, the center of the band is shifted to higher values (depending on the kinematic variables  $x_{Bj}$  and  $Q^2$ ). Besides the band, the hadronic final state of I-induced events exhibits a current jet coming from the outgoing current quark (denoted by  $q''$  in Fig. 1).

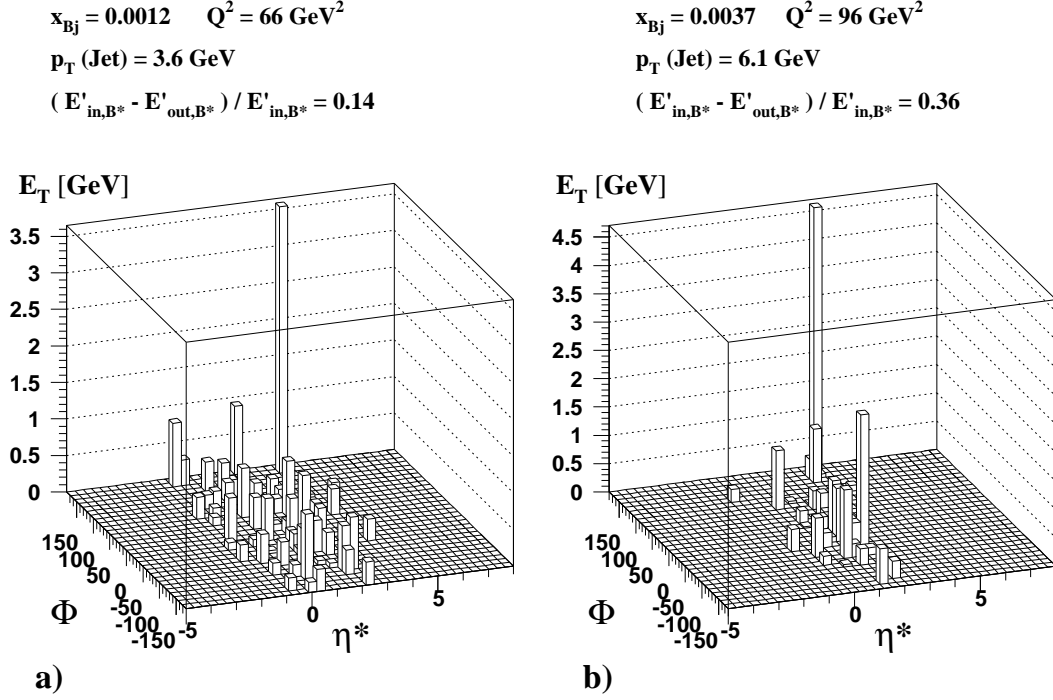


**Figure 3:** Transverse energy distributions in the  $\eta^*$ - $\Phi$ -plane (hCMS) of the hadronic final state particles of an I-induced process (shown for typical detector acceptance cuts). a) “Ideal” event signature. Besides the homogeneously populated “instanton-band” (at  $\eta^*$  between 0 and 2), the current jet at  $\eta^* \approx 3$ ,  $\Phi \approx 170^\circ$  is clearly visible. b) The homogeneous distribution of the hadrons in the instanton band is destroyed by a current jet with high  $p_T$ .

- **High multiplicity and “Flavour-democracy”**

In every I-induced event, one pair of quark and anti-quark of all  $n_f (= 3)$  flavours is simultaneously produced. In addition, a mean of  $\langle n_g \rangle^{(I)} \sim 1/\alpha_s \sim 3$  gluons is expected. Hence, for the phase space studied here, we find a mean number of partons of  $\mathcal{O}(10)$ , leading to a mean multiplicity of charged particles of  $\mathcal{O}(20)$  in every event. The actual number of hadrons produced mainly depends on the center of mass energy  $W_i$  accessible. Moreover, due to the democratic production of all (effectively massless) flavours, more mesons containing heavy quarks should be found in I-induced events than in normal DIS events. The detection of  $K^0$  mesons is experimentally most promising to exploit this feature.

- **High transverse energy**

While normal DIS events exhibit a mean value of 2 GeV of transverse energy per unit of  $\eta^*$  [24], for I-induced events a value of the order of 5 GeV in an  $\eta^*$  range of  $0 \lesssim \eta^* \lesssim 4$  is expected.

The ideal event topology described above (see also Fig. 3a) is quite often modified by simple kinematic effects. In the hCMS the sum of the transverse energy of the particles emerging from the I-subprocess and the  $p_T$  of the current jet has to be approximately balanced. In many cases

this leads to a destruction of the homogeneous  $\Phi$  distribution of the particles in the band. Fig. 3b gives an example for such an event topology. In general, with rising  $p_T$  of the current jet and lower particle multiplicities emerging from the I-subprocess, the band structure becomes less clearly visible.

In addition, the  $p_T$  of the jet strongly influences the relative  $\eta^*$  position of the jet and the instanton band. Fig. 4a demonstrates this effect for the parton final state. The mean  $\eta^*$  value of the current quark increases with rising  $p_T$  of the current quark, while the mean  $\eta^*$  values of the instanton band, outlined by the maximal and the mean ( $E_T$  weighted)  $\eta^*$  value of the partons coming from the I-subprocess, are decreasing. For hadrons (Fig. 4b) the  $\eta^*$  position of the current jet (which is reconstructed by a jet-finding algorithm, see section 4) and the  $E_T$  weighted mean  $\eta^*$  value of all particles not belonging to the jet (which we use as an estimator for the central position of the instanton band) show qualitatively the same behaviour<sup>5</sup>.

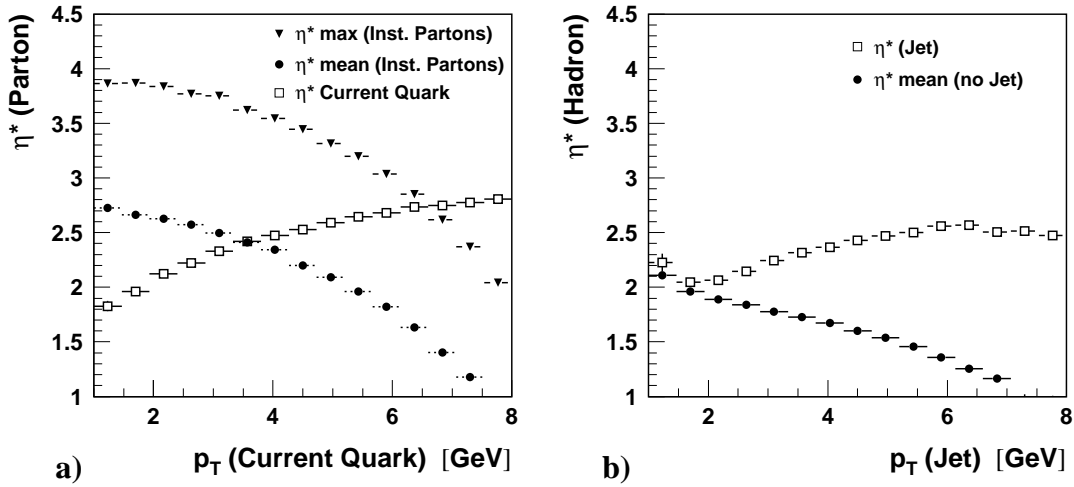


**Figure 4:** Evolution of the relative  $\eta^*$  position of the partons belonging to the  $I$ -subprocess and the current jet as a function of the  $p_T$  of the current quark and the current jet, respectively. In a) the instanton-band is outlined by the maximal and the  $E_T$  weighted mean  $\eta^*$  value of the partons coming from the  $I$ -subprocess. In b) the position of the band is characterized by the  $E_T$  weighted mean  $\eta^*$  value (calculated without the hadrons belonging to the jet).

In Fig. 4 and throughout this report, the kinematical range given in the context of Eq. (7) has actually been extended down to  $x_{Bj} = 10^{-4}$  with  $Q^2 = Sx_{Bj}y_{Bj} \geq 5 \text{ GeV}^2$ . On the one hand, within this enlarged kinematical region, there is the possible influence of non-planar graphs, which are not implemented in QCDINS. On the other hand, the hadronic final state topology of  $I$ -induced events will presumably not change dramatically, being mainly determined by the available phase space (see section 6). Since the cross section of  $I$ -induced events increases with

<sup>5</sup>The mean  $\eta^*$  values of the centre of the instanton band are lower than those for the parton final state, because for hadrons, particles of the proton remnant are also taken into account. Additionally, the mean  $\eta^*$  values for  $p_T(\text{current quark}) \lesssim 3 \text{ GeV}$  are not adequately reproduced on hadron level. In this range, the jet-finding algorithm mostly finds the “jet” within the hadrons belonging to the instanton band.



decreasing values of  $x_{Bj}$  and  $Q^2$  (as for normal DIS events), it is an experimental challenge to investigate the signal to background ratio also in this kinematical domain. In our extended study in Ref. [17] we shall restrict ourselves to the “fiducial” high- $Q^2$  regime (Eq. 4).

## 4 Reconstructing the kinematics of the I-subprocess

In this section we give a short summary of the possibility to reconstruct the kinematic variables of the I-subprocess which have been introduced in Fig. 1. A more detailed investigation can be found in [12]. The cross section of the I-subprocess is most sensitive to the values of  $Q'^2$  and  $x'$ . Therefore the possibility to reconstruct these variables would allow crucial tests of the predictions for the total cross section to be made, once I-induced topologies have been identified. Moreover, in order to reconstruct  $Q'^2$  and  $W_i$ , the separation of the current jet from the instanton band has to be as good as possible. We found the output of this procedure to be most useful in designing optimized observables in view of enhancing the separation power to normal DIS events. And finally, the reconstruction of  $Q'^2$  and  $\xi$  would allow a boost to the instanton center of mass frame to be performed.

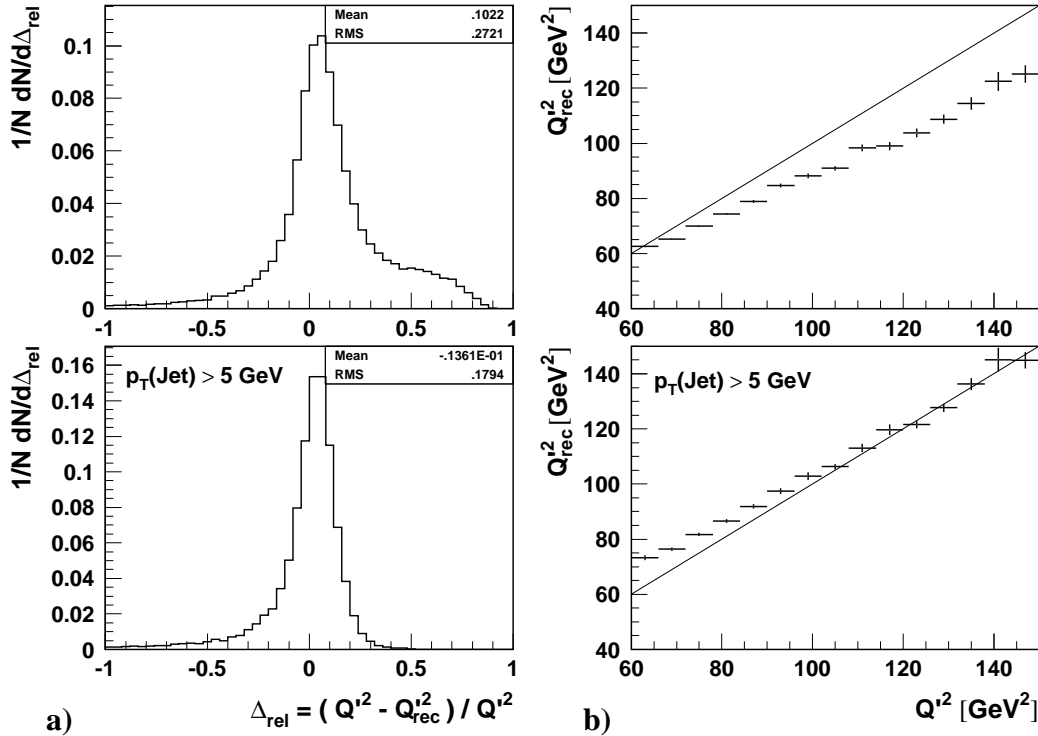


**Figure 5:** Reconstruction of  $Q'^2$  from the hadronic final state of I-induced events. a) Relative deviation of the true and the reconstructed value. b) Correlation between the mean value of the reconstructed  $Q'^2$  and the true value. In both cases the upper figure is without and the lower figure is with a  $p_T$  cut on the current jet.

The reconstruction of  $Q'^2$  is based on the assumption that the colour forces between the current jet and the rest of the partons, as modeled in the hadronisation phase, still allow the reconstruction of the current jet 4-vector. So  $q' = q - q''$  (cf. Fig. 1) and the reconstruction of  $Q'^2$  is performed by reconstructing the four-vector  $q''$  of the particles belonging to the current jet. To identify the current jet the cone algorithm [25, 26] is applied in the hCMS. A cone of radius  $R = 0.5$  (in the  $\eta^*$ - $\Phi$ -plane) turns out to perform best [12]. Motivated by the relative  $\eta^*$  position of the current quark and the instanton band (cf. Fig. 4), we additionally require the jet to fulfill  $\eta^* \geq \overline{\eta^*}$ , with  $\overline{\eta^*}$  being the  $E_T$ -weighted mean  $\eta^*$  value of all hadrons. The jet with the highest  $p_T$  is then assumed to be the most likely candidate for the current jet. Fig. 5 shows that this procedure gives a rather good reconstruction of  $Q'^2$ , especially, if the jet is required to have a  $p_T \geq 5$  GeV. This is also a reasonable choice in order to have a clear signal in the detector.

Once the current jet has been found, the hadrons belonging to the jet are removed from the final state and  $\overline{\eta^*}$  is recalculated with the remaining hadrons in order to get a good estimator for the center of the instanton band. For the calculation of  $W_i$  the four-vectors of all hadrons in a region left and right of  $\overline{\eta^*}$  are considered. A band of  $\overline{\eta^*} \pm 1.1$  gives the best possible results for the majority of events. This result is in agreement with the mean bandwidth visible in Fig. 4 as well as with the expectation for an isotropic event. The reconstruction of  $W_i$  is not perfect, though. If the bandwidth is determined for every single event (based on the known value of  $W_i$ ), a rather broad distribution is obtained, which peaks only weakly at  $\pm 1.1$ . In many events, slightly different bandwidths would be required for an optimal reconstruction of  $W_i$ . The procedure using the averaged bandwidth results in a quite large error of the reconstructed quantity of  $W_i$  of approx. 25 % (for  $p_T(jet) \geq 5$  GeV).

The variable  $x'$  can be calculated once  $Q'^2$  and  $W_i$  have been reconstructed. However, the errors of the  $Q'^2$  and the  $W_i$  reconstruction interact in such an unfavourable manner that a reconstruction of  $x'$  seems not very meaningful. Finally,  $\xi$  can be reconstructed via  $\hat{s}$ , which comprises the four-vectors of all the hadrons used for the reconstruction of  $Q'^2$  and  $W_i$ . The reconstruction of  $\xi$  works relatively well in a broad range of the variable. However, a reconstructed pair of  $q'$  and  $\xi$  leads to inconsistencies when trying to perform a boost to the instanton center of mass system in 50% of the cases, so that either variable would have to be corrected.

## 5 Search Strategies

A search strategy for I-induced processes is naturally based on the characteristic properties of the hadronic final state. The goal is to isolate - based on Monte Carlo predictions - an instanton enriched data sample by applying cuts on a set of observables. More than 30 observables have been investigated in [12]<sup>6</sup>. Fig. 6 demonstrates the procedure by which we measure the “separation power” of each observable. As an example, we investigate the distribution of the number

---

<sup>6</sup>For the results shown here additional cuts have been introduced to get a more realistic representation of the typical acceptance of a HERA detector. For this reason, some of the results presented here slightly deviate from those given in [12].

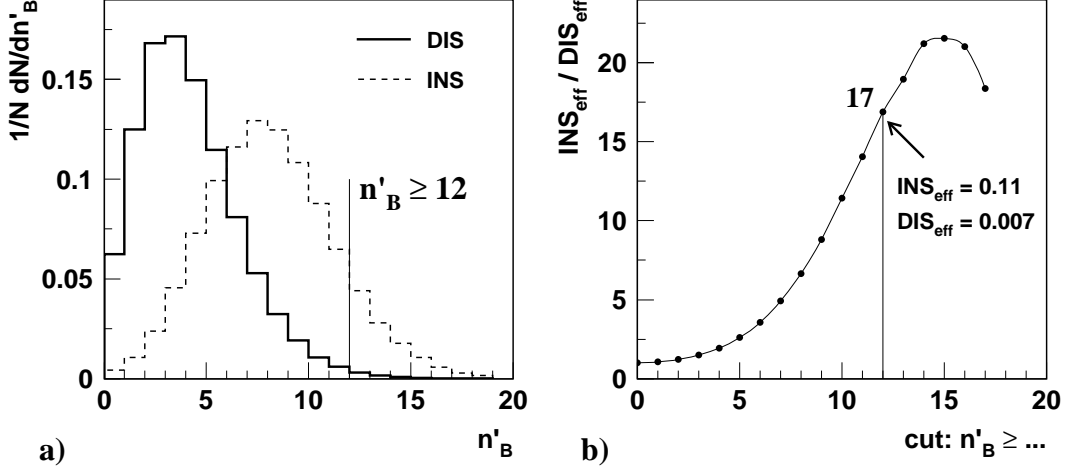


**Figure 6:** a) Shape normalized distributions of the number of charged particles in the instanton band  $n'_B$  (without the hadrons belonging to the current jet) for normal DIS and I-induced events. b) Separation power ( $:= INS_{eff}/DIS_{eff}$ ) after applying cuts in  $n'_B$  for every possible cut. Explicitly shown are the values for the cut with the highest separation power, which fulfills the requirement of a remaining instanton efficiency of 10 %.

of charged particles  $n'_B$ , where the index “B” indicates that we consider only particles of the instanton band ( $\overline{\eta^*} \pm 1.1$ ), and the prime indicates that the hadrons belonging to the current jet are not considered. Starting from shape normalized distributions for normal DIS and I-induced events (Fig. 6a), we calculate the ratio of efficiencies for I-induced over normal DIS events for each possible cut value (Fig. 6b). We require a minimum instanton efficiency, which we (arbitrarily) set to 10 %. The cut  $n'_B \geq 12$  leads to a ratio of the efficiencies, or - in our terminology - to a separation power of  $INS_{eff}/DIS_{eff} \simeq 17$ . In general, applying cuts in only *one* observable typically leads to a separation power not higher than  $\mathcal{O}(20)$  (c.f. [12]).

An obvious improvement in separating I-induced from normal DIS events is obtained by the combination of cuts in several observables. However, since most of the observables are highly correlated, the naive combination of the best one-dimensional cuts quite often fails in enhancing the separation power. On the contrary, in some cases it would even lead to a reduction of the separation power, an effect for which we give an example now. Since in any I-induced event at least one  $s\bar{s}$  pair is produced, an excess in the number of neutral kaons in comparison to normal DIS events is expected. Fig. 7a shows, however, that this excess is almost not visible for events with higher particle multiplicities. Investigating the correlation between the mean number of kaons and the number of charged particles (Fig. 7b), we find the expected excess for relatively low particle multiplicities, only. For some value of  $n'_B$ , the number of neutral kaons produced in normal DIS events actually *exceeds* the number produced in I-induced events. Applying cuts requiring a high value of  $n'_B$  together with a large number of neutral kaons would therefore reduce the separation power. Since in addition the number of kaons produced rather strongly depends on variations of the underlying MC model, kaons play no role in our multi-dimensional cut-scenario. The study of strange mesons or baryons (notably  $\Lambda$ 's) could, however, play a major role once an

instanton enriched sample is experimentally isolated from the data.

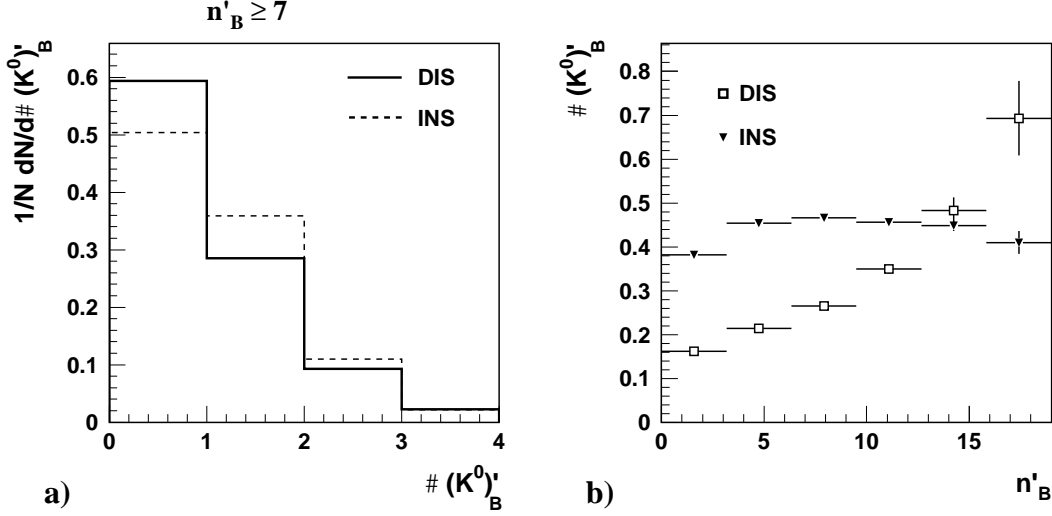


**Figure 7:** a) Shape normalized distributions of the number of neutral kaons in the instanton band for normal DIS and I-induced events, while applying the additional cut  $n'_B \geq 7$ . b) Correlation between the mean number of neutral kaons and the number of charged particles.

Based on a study of the correlations and mutual influences of different cuts, we now introduce a set of six observables which are able to enhance the separation power from  $\mathcal{O}(20)$  to  $\mathcal{O}(130)$ . Fig. 8 shows these observables together with the cuts applied in each observable, indicated by the lines and the corresponding arrows<sup>7</sup>.

This cut-scenario has been established in a study of what we call “reference” (or default) Monte Carlos. For the (default) simulation of normal DIS events we use the Lund MC generator ARIADNE ([27], including Pomeron exchange), which includes the Colour Dipol Model (CDM, [28, 29, 30]) to describe higher order perturbative QCD radiation. Although not perfect, ARIADNE presently gives the best description of the properties of the hadronic final state at HERA [31, 32]. For the simulation of I-induced events we use QCDINS [9, 18], which is based on the matrix element of the I-subprocess and interfaced by default to HERWIG [19] for the simulation of parton showers, fragmentation and particle decays (see section 2). The shaded band shown in Fig. 8 stems from variations of the Monte Carlo simulations (see section 6)<sup>8</sup>.

All distributions presented here are normalized to the number of events. Fig. 8a shows the distribution of the  $p_T$  of the current jet, i.e. the jet with the highest  $p_T$ , for which  $\eta^*(jet) \geq \overline{\eta^*}$  holds. The distribution for I-induced events is rather flat for  $p_T$  values of 1 to  $\sim 7$  GeV, while for normal DIS events the spectrum steeply falls towards higher  $p_T$ . Fig. 8b shows the distribution of  $Q'^2_{rec}$ , a quantity which has no direct physical interpretation for normal DIS events, but which exhibits a rather good separation power (especially in correlation to  $n'_B$ , c.f. [12]). The

<sup>7</sup> An explicit listing of these cuts is given in Figs. 12 and 13.

<sup>8</sup> A list of *all* variations used in creating the shaded band in Fig. 8 is given in Fig. 12 and Fig. 13.

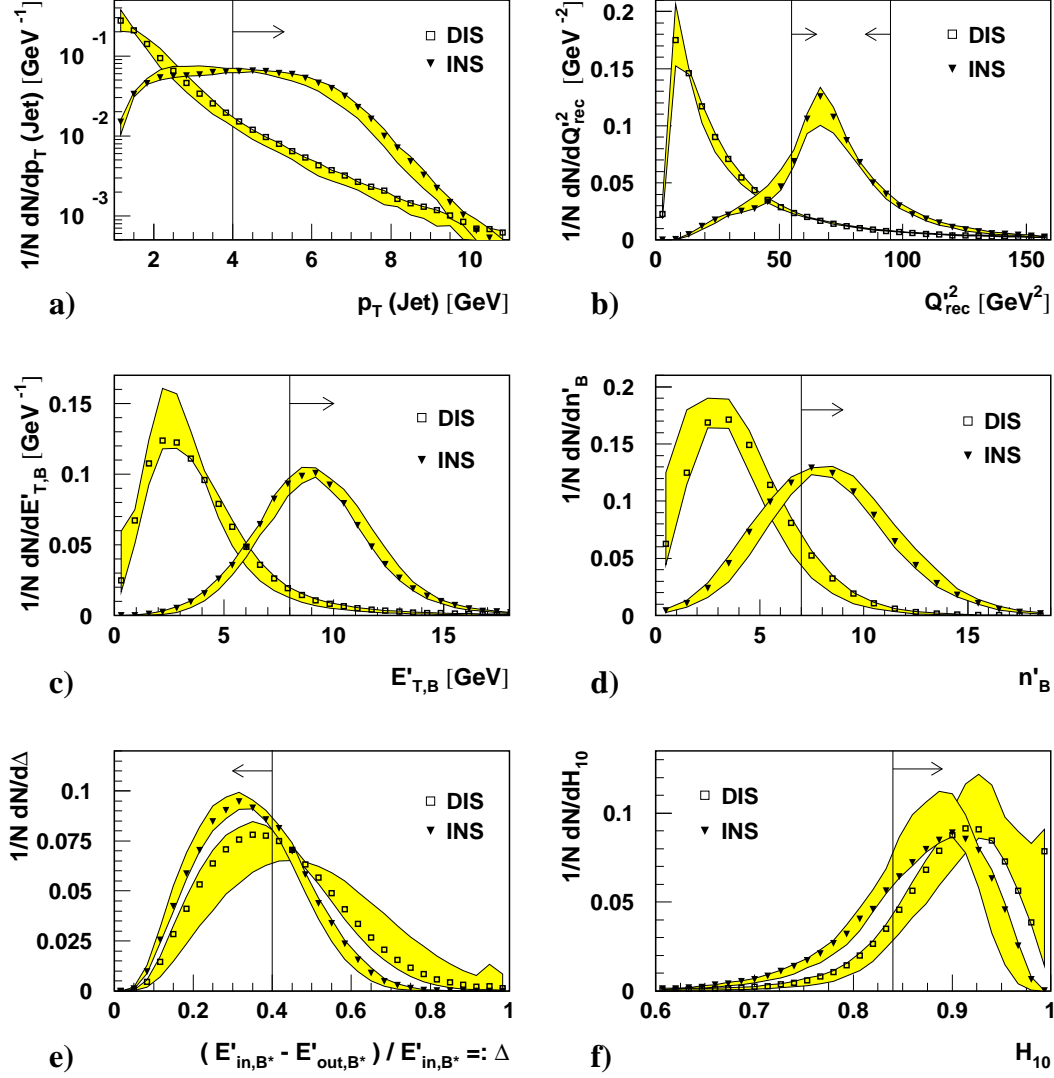


**Figure 8:** Distributions of various observables for normal DIS and I-induced processes. Shown are the distributions for the “reference Monte Carlos” (INS markers = QCDINS + HERWIG, DIS markers = ARIADNE, including Pomeron exchange) and their variations (shaded band) resulting from the choice of different models or the variation of parameters of a model (c.f. Fig. 12 and Fig. 13). The lines and the corresponding arrows show the cut applied in each of the observables, with the arrows pointing in the direction of the allowed region.

distribution of the transverse energy and of the charged particles in the instanton band ( $\overline{\eta^*} \pm 1.1$ ) is displayed in Fig. 8c and in Fig. 8d. Both distributions reflect the high partonic (and following hadronic) activity in the I-subprocess. The observables depicted in Fig. 8e and 8f make use of the shape of I-induced events which is supposed to be more isotropic than that of normal DIS events. Fig. 8e gives the distribution of the relative  $E_{\text{in}}-E_{\text{out}}$  difference, a quantity, which measures the  $E_T$  weighted  $\Phi$  isotropy of an event (for a detailed description see [12, 33]). The

more homogeneous the transverse energy is distributed in  $\Phi$ , the lower the relative  $E_{in}-E_{out}$  difference becomes. Again, we investigate this quantity in the band<sup>9</sup>, after subtracting the hadrons belonging to the current jet. Normal DIS events seem to exhibit a surprisingly low value of this quantity, implying a rather isotropic  $\Phi$  distribution of the remaining hadrons. However, this behaviour strongly varies with the MC model used as is illustrated by the shaded band. This similarity of the distributions for normal DIS and I-induced events disappears for events with high  $E_T$  as expected and as demonstrated in Fig. 9a. Here, normal DIS events exhibit the expected jet-like structure with low ( $\Phi$ ) isotropy, while I-induced events remain as isotropic as before. Finally, in Fig. 8f, we investigate the distributions of the first Fox-Wolfram moment

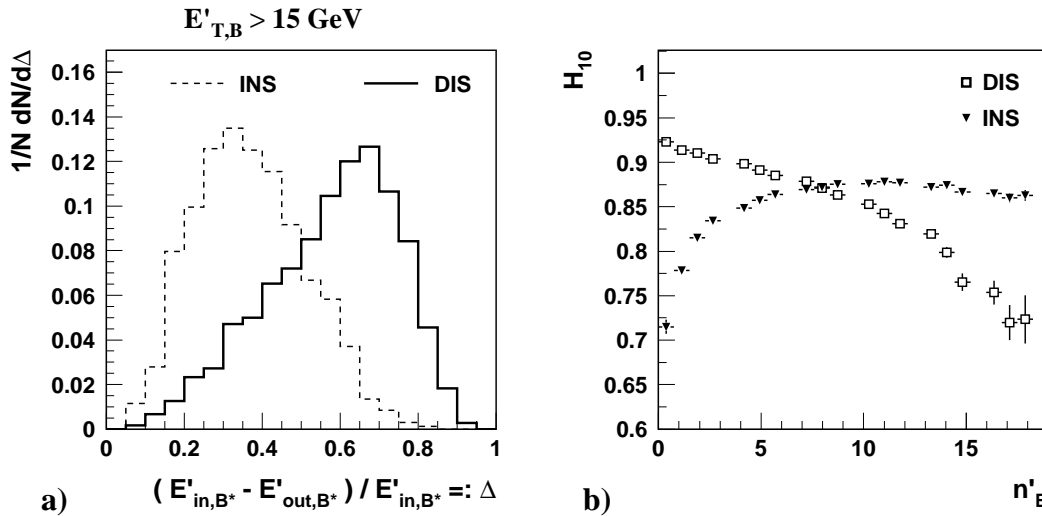


**Figure 9:** a) Shape normalized distributions of the relative  $E_{in}-E_{out}$  difference (in the instanton band, without jet hadrons) for normal DIS and I-induced events, while applying the additional cut  $E'_{T,B} \geq 15$  GeV. b) Correlation between the mean first Fox-Wolfram moment  $H_{10}$  and the number of charged particles  $n'_B$  (in the instanton band, without jet hadrons).

$H_{10}$  [34] (normalized to the zeroth moment), an event shape variable which is independent of the axis chosen to calculate it. The Fox-Wolfram moments, in general, seem to perform better than all other studied event shape variables (like sphericity, thrust etc) in separating normal DIS from I-induced events (c.f. [12]). To understand, why the cut indicated by the arrow in Fig. 8f improves the separation power, the correlation between  $H_{10}$  and  $n'_B$  has to be taken into account (Fig. 9b). For high charged particle multiplicities, the mean value of  $H_{10}$  of normal DIS events lies *below* that of I-induced events so that cutting at higher values of  $H_{10}$  is reasonable<sup>10</sup>.

The multi-dimensional cut-scenario indicated in Fig. 8 leads to a separation power of  $INS_{eff}/DIS_{eff} \simeq 130$ , with the remaining efficiencies  $INS_{eff} \simeq 10\%$  and  $DIS_{eff} \simeq 0.08\%$ .

<sup>9</sup>The separation obtained with this quantity can be enhanced by taking into account all hadrons in a broader range in  $\eta^*$  ( $\overline{\eta^*} \pm 1.6$ ). This is indicated by the index “B\*”.

<sup>10</sup>The peak of the  $H_{10}$  distribution at  $H_{10} \simeq 1$  (Fig. 8f) is due to diffractive events (simulated by the Pomeron exchange or the SCI mechanism) which usually have very low multiplicities ( $n \leq 4$ ).

If we extrapolate the prediction for the cross section given in Eq. (7) to the kinematical range investigated in this report ( $x_{\text{Bj}} \geq 10^{-4}$ ,  $Q^2 \geq 5 \text{ GeV}^2$ ,  $0.1 < y < 0.6$ ), we find  $\sigma_{\text{HERA}}^{(I)} \simeq 215 \text{ pb}$ , and  $\sigma_{\text{HERA}}^{(I)} \simeq 22 \text{ pb}$  after applying all cuts, respectively. For  $\mathcal{L} \simeq 30 \text{ pb}^{-1}$ , one finds for the number of I-induced events  $N_{\text{INS}} \simeq 670$ , while  $N_{\text{DIS}} \simeq 1810$  of normal DIS events are expected. This implies an  $\mathcal{O}(13)\sigma$  effect when compared to the merely statistical DIS expectation.

## 6 Dependencies on MC models

In this section, we investigate how the final-state observables depend on the MC models used for the simulation of I-induced as well as normal DIS events. In the default version of QCDINS the cluster fragmentation model [35] is used. Given the large number of  $\mathcal{O}(10)$  partons produced in a narrow  $\eta^*$ -interval by the I-subprocess, a thorough investigation of hadronization alternatives would be very desirable, since so far there is little experience with such configurations of high parton densities. In the following study we start with what is available in this context. For a selection of important distributions, Fig. 10 illustrates the effects of using the Lund string model [22, 36, 37] as implemented in JETSET [22] for fragmentation. The markers show the default implementation of QCDINS, while the shaded band reflects variations of QCDINS + JETSET, arising from different tunings of the JETSET parameters, which are obtained from studying the hadronic final state in  $e^+e^-$  collisions [38]. Fig. 10a shows that the mean number of charged hadrons produced in an I-induced event slightly increases when using string fragmentation. For the number of neutral kaons (cf. Fig. 10b), however, a significant difference to the values obtained in the cluster fragmentation model is found. The Figs. 10c and d basically are a direct result of the larger number of hadrons produced, i.e. a slightly larger mean value of the transverse energy and a slightly more ( $\Phi$ ) isotropic distribution of the particles produced in an I-induced event. In general, we find that the prediction for the properties of the hadronic final state of I-induced events depends only weakly on the choice of the model used to simulate the hadronisation. This statement is supported by studying the effects of the HERWIG tuning, as suggested in [31]. Two parameters of the cluster fragmentation model influencing the maximum allowed cluster mass (CLMAX) and the mass distribution of the split clusters (PSPLT) are changed in the tuned HERWIG version. In Fig. 11 we find, that this modifications strongly influence the distributions for normal DIS events<sup>11</sup>. On the contrary, the distributions of I-induced events only show rather slight variations<sup>12</sup>. Besides the influence of the  $p_T$  of the current jet, the hadronic final state of I-induced events seems to be mainly determined by the dynamics of the I-subprocess, and by the available phase space in  $x'$  and  $Q'$ .

Besides the parameters or models determining the hadronisation, we also varied the structure function of the proton from CTEQ4L [39] (which we used as default) to MRSH [40] in the simulation of I-induced events. This variation results in a small decrease of the total cross section,

<sup>11</sup>An exception is the number of neutral kaons, which seems to be not influenced by this parameter tuning.

<sup>12</sup>One exception to this general behaviour is the distribution of the first Fox-Wolfram moment, presented in Fig. 8f, which shows rather strong variations when using JETSET or the untuned HERWIG instead of the tuned HERWIG for the hadronisation of I-induced events.

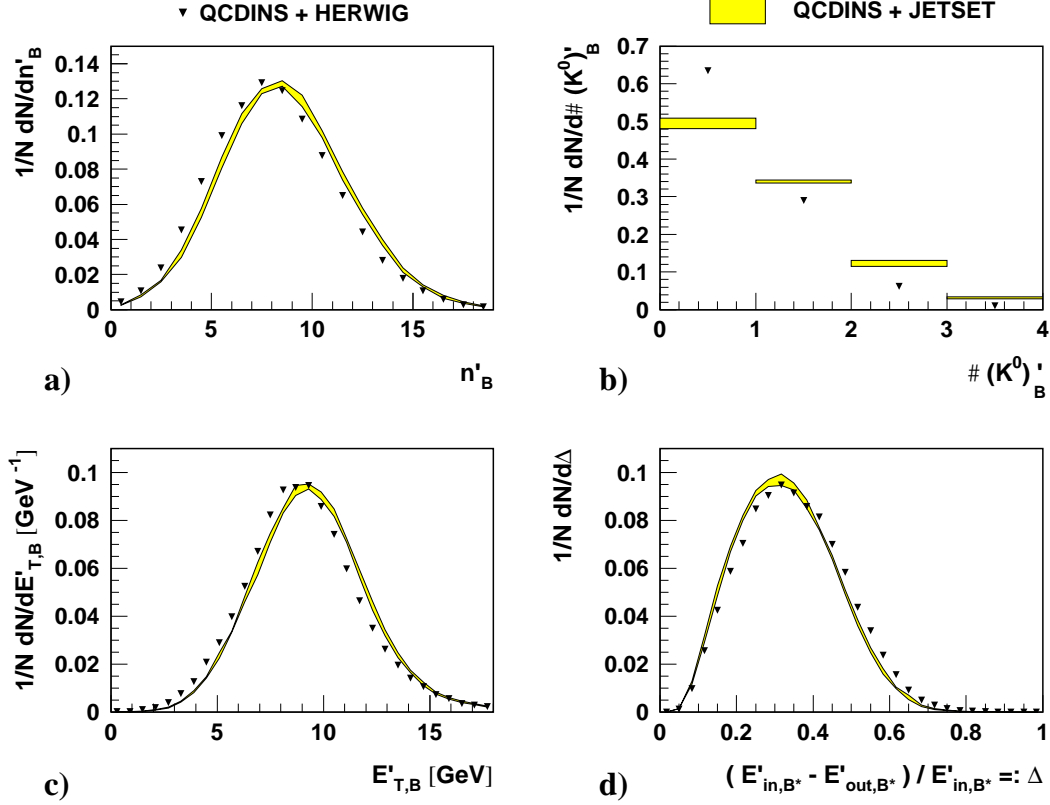


**Figure 10:** Comparison of different models to simulate the hadronisation of I-induced events with respect to their effect on a selection of distributions. The markers represent the default QCDINS implementation (QCDINS + HERWIG (tuned) = cluster fragmentation), while the shaded band represents QCDINS plus Lund string fragmentation (as implemented in JETSET) with different tunings applied (see text).

but shows almost no visible effect in the distributions of the hadronic final state observables. Finally, we varied the scale  $\Lambda_{\overline{\text{MS}}}^{(3)}$  within its experimental uncertainty as explained in section 3. Besides the expected strong influence on the cross section of I-induced events, the lower value of  $\Lambda_{\overline{\text{MS}}}^{(3)}$  has the effect of slightly enhancing the charged particle multiplicity, while the higher value leads to slightly lower multiplicities. This effect can be easily explained as an increase or decrease in the mean gluon multiplicity which is proportional to  $1/\alpha_s$  and thus increases with decreasing  $\Lambda_{\overline{\text{MS}}}^{(3)}$ .

Fig. 12 shows the influence of all the variations of the simulation of I-induced events on the separation power of our multi-dimensional cut-scenario (explicitly given on top of the figure). For the simulation of normal DIS events we use (our default) MC model ARIADNE (with Pomeron exchange) as reference. As mentioned, the application of all cuts leads to a remaining DIS efficiency of  $8 \cdot 10^{-4}$  or, respectively, a number of events of  $N_{DIS} \simeq 1810$ , when normalized to  $\mathcal{L} \simeq 30 \text{ pb}^{-1}$ . The variations used in the modeling of I-induced events are sorted according to the separation power. The corresponding efficiencies range from approx. 9% to 11%. After



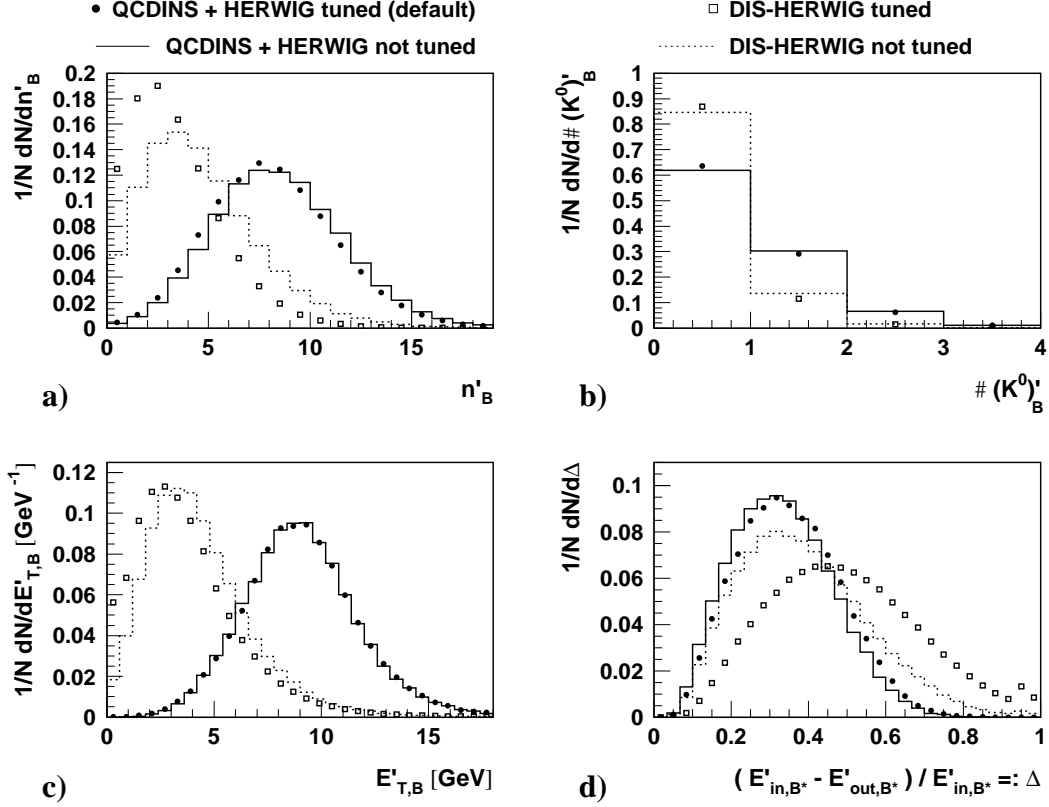


**Figure 11:** Comparison of the influence of HERWIG tuning for normal DIS and I-induced events with respect to its effect on a selection of distributions.

normalization to the luminosity given above, one finds that the numbers of I-induced events remaining vary only slightly between  $N_{INS} \simeq 550$  and  $N_{INS} \simeq 670$ . Because of its strong influence on the cross section for I-induced events, the obvious exception to this is the variation of the scale  $\Lambda_{\overline{\text{MS}}}^{(3)}$ , which results in the worst and the best prediction for the remaining number of events, namely  $N_{INS} \simeq 140$  and  $N_{INS} \simeq 1930$ , respectively.

Another important aspect to investigate is the dependence of the separation power on variations of the MC models used to simulate normal DIS events. To this end, three different MC generators are used in our study: ARIADNE, LEPTO [41] and HERWIG. All generators are operated in the “tuned version”, i.e. with parameter settings obtained in optimizing the description of the hadronic final state at HERA [31]. For the generators ARIADNE and LEPTO, the simulation of diffractive events (modeled via the Pomeron exchange and the SCI-mechanism, respectively) has each been turned on and off. Fig. 13 shows the influence of these variations on the separation power of our multi-dimensional cut-scenario. This time, we fix the simulation of I-induced events to be described by our reference MC model QCDINS + HERWIG (tuned). The separation powers using LEPTO or ARIADNE turn out to be rather similar, while HERWIG gives a significantly different result. Quite remarkably, the expected difference in separation power, arising from the usage of different models for hadronisation, is even more pronounced in the tuned version of HERWIG

Cuts:

$$55 \text{ GeV}^2 < Q_{\text{rec}}^2 < 95 \text{ GeV}^2$$

$$p_T(\text{Jet}) > 4 \text{ GeV}$$

$$E'_{T,B} > 8 \text{ GeV}$$

$$(E'_{\text{in},B^*} - E'_{\text{out},B^*}) / E'_{\text{in},B^*} < 0.4$$

$$H_{10} > 0.84$$

$$n'_B \geq 7$$

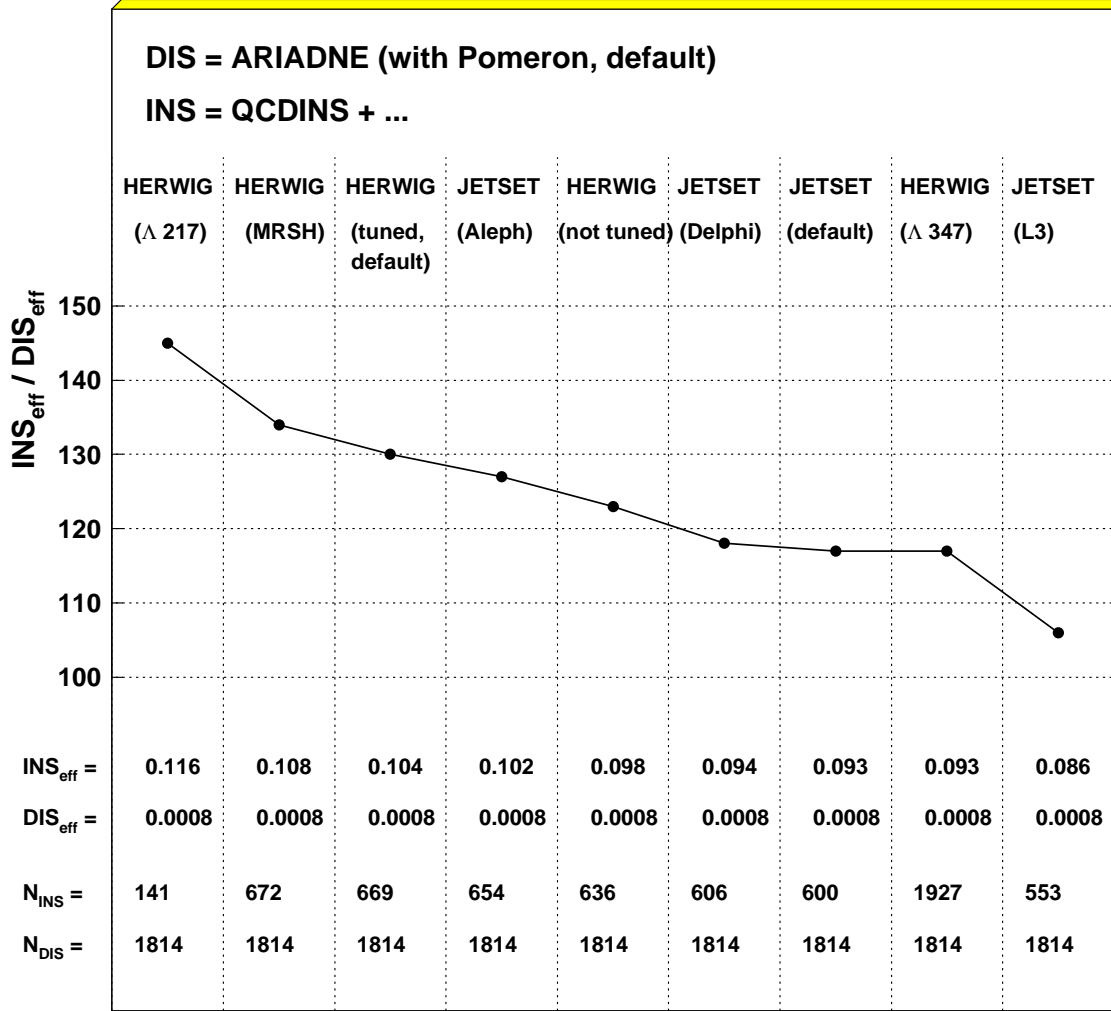


**Figure 12:** Dependence of the separation power ( $INS_{\text{eff}}/DIS_{\text{eff}}$ ) of a multidimensional cut-scenario on the variation of MC models and parameters used to simulate I-induced events. The corresponding efficiencies are listed, as are the numbers of events remaining (assuming an integrated luminosity of  $\mathcal{L} \simeq 30 \text{ pb}^{-1}$ ).

(which was tuned according to the same distributions as ARIADNE and LEPTO, c. f. [31]). To demonstrate this effect, the results obtained using the untuned HERWIG implementation are additionally presented in Fig. 13. The obtained efficiencies result (for  $\mathcal{L} \simeq 30 \text{ pb}^{-1}$ ) in numbers of remaining normal DIS events ranging from  $N_{\text{DIS}} \simeq 930$ , at  $DIS_{\text{eff}} \simeq 4 \cdot 10^{-4}$  when using HERWIG (tuned), to  $N_{\text{DIS}} \simeq 2025$ , at  $DIS_{\text{eff}} \simeq 9 \cdot 10^{-4}$ , when using ARIADNE (without Pomeron exchange). For I-induced events we find the already quoted value of  $N_{\text{INS}} \simeq 669$ .

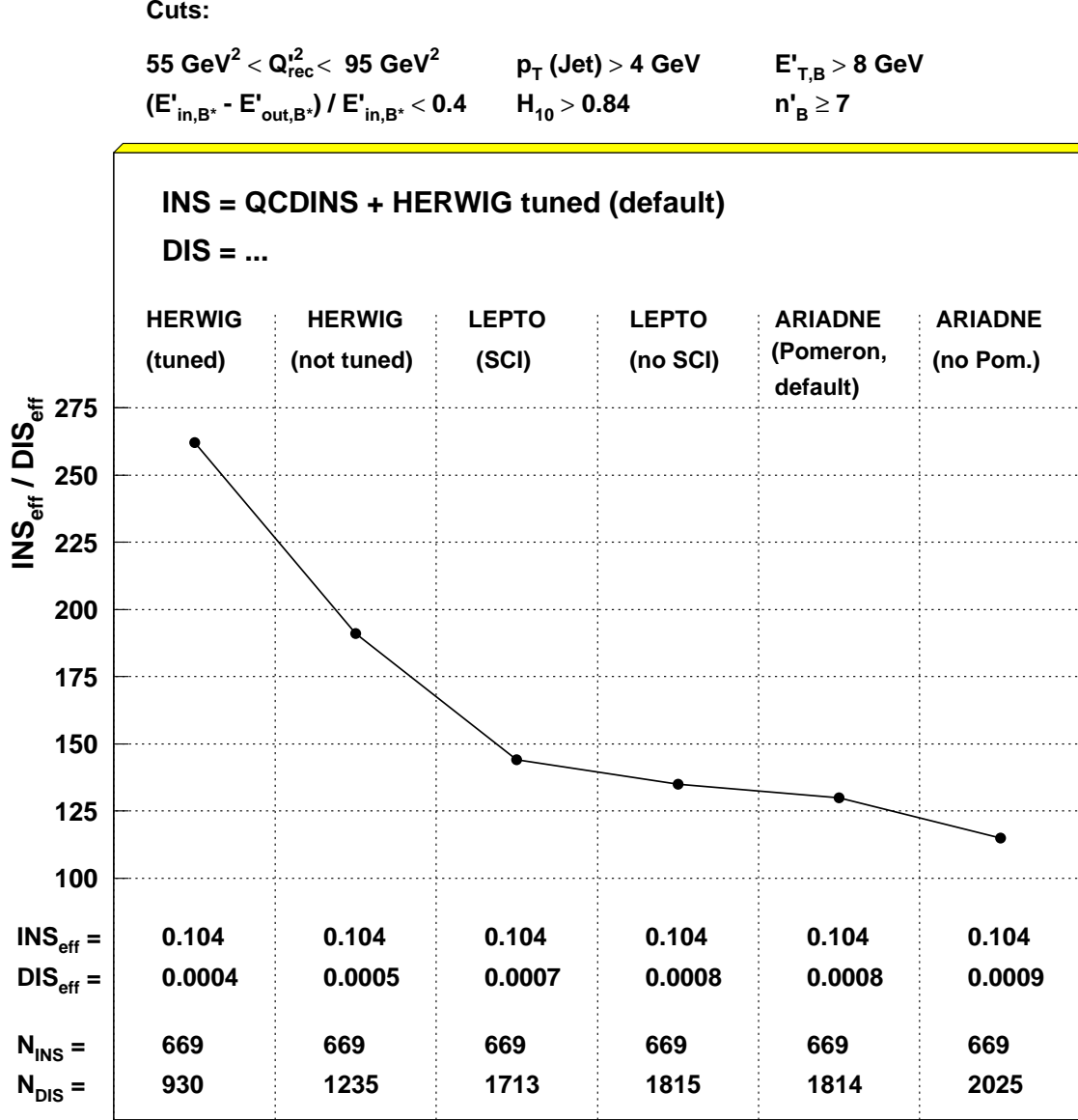


**Figure 13:** Dependence of the separation power ( $INS_{\text{eff}}/DIS_{\text{eff}}$ ) of a multidimensional cut-scenario on the variation of the MC generator used to simulate normal DIS events. The corresponding efficiencies are listed, as are the numbers of events remaining (assuming an integrated luminosity of  $\mathcal{L} \simeq 30 \text{ pb}^{-1}$ ).

## 7 Conclusion

The experimental discovery of instanton-induced processes in DIS at HERA would be a novel, non-perturbative manifestation of QCD, and therefore be of basic significance. Based on the characteristic hadronic final state of I-induced events, we found a set of six observables that exhibit a good “separation-power” to normal DIS events. In our best cut-scenario, normal DIS events

are suppressed by a factor of  $8 \cdot 10^{-4}$ , while 10% of I-induced events survive. For  $\mathcal{L} \simeq 30 \text{ pb}^{-1}$  and the nominal value of the theoretical cross section, this results in a predicted number of  $N_{INS} \simeq 670$ , for I-induced events, while  $N_{DIS} \simeq 1810$  of normal DIS events are expected. Within the “bandwidth” of variations considered, the systematic uncertainties arising from the modeling of I-induced events are surprisingly small. In this case, the structure of the hadronic final state seems to be mainly determined by the dynamics of the I-subprocess and by the available phase space in  $x'$  and  $Q'$ . On the contrary, the simulation of normal DIS events is found to be much more sensitive to the variation of model parameters. Thus, a better understanding of the tails of distributions for normal DIS events turns out to be quite important.

## 8 Acknowledgments

We would like to thank H. Jung for his help to interface QCDINS with JETSET.

## References

- [1] A. BELAVIN, A. POLYAKOV, A. SCHWARZ AND YU. TYUPKIN, *Phys. Lett. B* 59 (1975) 85.
- [2] G. 'T HOOFT, *Phys. Rev. Lett.* 37 (1976) 8.
- [3] G. 'T HOOFT, *Phys. Rev. D* 14 (1976) 3432.
- [4] G. 'T HOOFT, *Phys. Rev. D* 18 (1978) 2199 (Erratum).
- [5] S. ADLER, *Phys. Rep.* 177 (1969) 2426.
- [6] J. BELL AND R. JACKIW, *Nuovo Cimento* 51 (1969) 47.
- [7] W. BARDEEN, *Phys. Rep.* 184 (1969) 1848.
- [8] A. RINGWALD AND F. SCHREMPP, In *Quarks '94* (Vladimir, Russia, 1994), D. Grigoriev et al., Eds., Proc. of the 8th Int. Seminar, pp. 170–193, hep-ph/9411217.
- [9] M. GIBBS, A. RINGWALD AND F. SCHREMPP, In *Proc. DIS 1995* (Paris, 1995), J.-F. Laporte and Y. Sirois, Eds., pp. 341–344, hep-ph/9506392.
- [10] A. RINGWALD AND F. SCHREMPP, In *Quarks '96* (Yaroslavl, Russia, 1996), V. Matveev et al., Eds., vol. I of *Proc. of the 9th Int. Seminar*, pp. 29–54, hep-ph/9610213.
- [11] A. RINGWALD AND F. SCHREMPP, In *Proc. DIS 97* (Chicago, 1997), J. Repond and D. Krakauer, Eds., pp. 781–786, hep-ph/9706399.
- [12] J. GERIGK, *Dipl. Thesis University of Hamburg (unpublished) and MPI-PhE/98-20* (Nov. 1998).
- [13] I. BALITSKY AND V. BRAUN, *Phys. Lett. B* 314 (1993) 237.
- [14] S. MOCH, A. RINGWALD AND F. SCHREMPP, *Nucl. Phys. B* 507 (1997) 134.

- [15] A. RINGWALD AND F. SCHREMPP, *Phys. Lett. B* 438 (1998) 217.
- [16] S. MOCH, A. RINGWALD AND F. SCHREMPP, *in preparation*.
- [17] T. CARLI, J. GERIGK, A. RINGWALD AND F. SCHREMPP, *in preparation*.
- [18] A. RINGWALD AND F. SCHREMPP, *in preparation*.
- [19] G. MARCHESINI ET AL., *Comp. Phys. Commun.* 67 (1992) 465.
- [20] A. RINGWALD AND F. SCHREMPP, *hep-lat/9903039*, to appear in *Phys. Lett. B* (1999).
- [21] PARTICLE DATA GROUP, R.M. BARNETT *et al.*, *Phys. Rev. D* 54 (1996) 1.
- [22] T. SJÖSTRAND, *Comp. Phys. Commun.* 82 (1994) 74.
- [23] D. SMITH AND M. TEPPER, *Phys. Rev. D* 58 (1998) 014505.
- [24] H1 COLLAB., S. AID ET AL., *Phys. Lett. B* 356 (1995) 118.
- [25] L. POZO, *University of Cambridge, RALT-002* (1993).
- [26] CDF COLLAB., F. ABE ET AL., *Phys. Rev. D* 45 (1992) 1458.
- [27] L. LÖNNBLAD, *Comp. Phys. Commun.* 71 (1992) 15.
- [28] G. GUSTAFSON AND ULF PETTERSON, *Nucl. Phys. B* 306 (1988) 741.
- [29] G. GUSTAFSON, *Phys. Lett. B* 175 (1986) 453.
- [30] B. ANDERSSON ET AL., *Z. Phys. C* 43 (1989) 625.
- [31] N. BROOK ET AL., In *Future Physics at HERA* (Hamburg, 1996), G. Ingelman, A. D. Roeck, and R. Klanner, Eds., vol. 1, p. 613.
- [32] N. BROOK ET AL., In *these proceedings* (1999).
- [33] M. GIBBS ET AL., In *Future Physics at HERA* (Hamburg, 1996), G. Ingelman, A. D. Roeck, and R. Klanner, Eds., vol. 1, p. 509.
- [34] G. FOX AND S. WOLFRAM, *Nucl. Phys. B* 149 (1979) 413.
- [35] B. WEBBER, *Nucl. Phys. B* 238 (1984) 492.
- [36] B. ANDERSSON, G. GUSTAFSON, G. INGELMAN AND T. SJÖSTRAND, *Phys. Rep.* 97 (1983) 33.
- [37] B. ANDERSSON, G. GUSTAFSON AND B. SÖDERBERG, *Z. Phys. C* 20 (1983) 317.
- [38] I. KNOWLES ET AL., In *Physics at LEP2* (Geneva, 1995), G. Altarelli, T. Sjöstrand, and F. Zwirner, Eds., vol. 2, p. 103.
- [39] H.L. LAI ET AL, *Phys. Rev. D* 55 (1997) 1280.
- [40] A.D. MARTIN, W.J. STIRLING AND R.G. ROBERTS, In *Quantum Field Theory and Theoretical Aspects of HEP* (1993), B. Geyer and E. Ilgenfritz, Eds., p. 11.
- [41] G. INGELMAN, A. EDIN AND J. RATHSMAN, *Comp. Phys. Comm.* 101 (1997) 108.